Localized Dynamic Light Scattering: A New Approach to Dynamic Measurements in Optical Microscopy

A. Meller,* R. Bar-Ziv,* T. Tlusty,# E. Moses,* J. Stavans,* and S. A. Safran#
*Department of Physics of Complex Systems and #Department of Materials and Interfaces, The Weizmann Institute of Science, Rehovot 76100, Israel

ABSTRACT We present a new approach to probing single-particle dynamics that uses dynamic light scattering from a localized region. By scattering a focused laser beam from a micron-size particle, we measure its spatial fluctuations via the temporal autocorrelation of the scattered intensity. We demonstrate the applicability of this approach by measuring the three-dimensional force constants of a single bead and a pair of beads trapped by laser tweezers. The scattering equations that relate the scattered intensity autocorrelation to the particle position correlation function are derived. This technique has potential applications for measurement of biomolecular force constants and probing viscoelastic properties of complex media.

INTRODUCTION

The development of new techniques of micromanipulation that are able to probe the behavior of microscopic objects at length scales comparable to those of single macromolecules has opened new horizons for research in fields ranging from physics to biology. Optical tweezers (Ashkin, 1980; Ashkin et al., 1997; Svoboda and Block, 1994; Simmons et al., 1996) have allowed researchers to measure the elastic properties of single DNA molecules and their behavior as model polymers, measure the forces exerted by single motor proteins and enzymes such as RNA polymerase, probe forces in colloidal crystals, and test basic notions of statistical physics, such as transport in thermal ratchets and escape from potential barriers (Kuo and Sheetz, 1993; Svoboda et al., 1993, 1994; Finer et al., 1994; Yin et al., 1995). In many of these experiments there has been a recurrent need to detect minute motions or displacements, from which forces or other properties of interest can then be extracted. This has been done, for example, by monitoring the position of particles by video, by using interferometric methods, or by tracking displacements with multielement semiconductor devices.

We have recently proposed the technique of localized dynamic light scattering (LDLS) for the study of dynamical properties of single objects at the nanometer level (Bar-Ziv et al., 1997). LDLS differs from other well-established dynamic light scattering techniques (DLS) in a number of key aspects. In a typical homodyne DLS experiment, one illuminates a large number of particles with a nearly homogeneous field of light (Berne and Pecora, 1976; Chu, 1991). Temporal light intensity fluctuations at a distant detector arise from the interference of the scattered fields, whose relative phases shift due to the thermally induced motion of the scatterers. Intensity fluctuations induced by changes in the number of particles within the scattering volume are negligible because of their large number. In contrast, LDLS is based on scattering by a single object in a highly inhomogeneous field of light. The scatterer can be a simple particle such as a solid bead or a droplet, or an object with internal degrees of freedom, such as a cell organelle or membrane. The illumination field can be produced, for example, by focusing a laser beam with a microscope objective, or by an evanescent field. An optical fiber placed in closed proximity to the object collects the light that the object scatters and transfers it to a photodetector whose signal is fed to a digital autocorrelator for the calculation of the temporal autocorrelation function.

In this paper we present the main principles of the LDLS technique. The outline of this paper is as follows. In the next section we obtain theoretical expressions for the temporal intensity autocorrelation function for a focused beam. This is followed by a description of our experimental setup, and in the Results we illustrate the technique by applying it to beads trapped in a potential well formed with optical tweezers. Finally, we present a summary and discuss possible extensions and limitations of LDLS.

THEORY

In this section we establish the theoretical framework for understanding the scattering autocorrelation function (ACF) from a single particle in an inhomogeneous light field. We consider a rigid particle with no internal degrees of freedom, moving inside an intensity distribution $I(\vec{r})$ that is peaked at $\vec{r} = 0$. As the particle moves away from the origin, it scatters less light according to its position along the intensity gradient. Therefore, the scattered intensity $I_s(\vec{r})$, which is proportional to $I(\vec{r})$, is directly related to the dynamics of the center of mass of the particle $\vec{R}(t)$. This implies that the

Received for publication 18 July 1997 and in final form 4 December 1997.

Address reprint requests to Dr. Amit Meller, Genome Center, Department of Molecular Genetics, Weizmann Institute of Science, 76100 Rehovot, Israel. Tel.:972-8-9343686;Fax:972-8-9344112;E-mail:feamit@weizmann.weizmann.ac.il.

Dr. Bar-Ziv's present address is Center for Studies in Physics and Biology, The Rockefeller University, 1230 York Ave., New York, NY 10016.

0006-3495/98/03/1541/08 $2.00

time dependence of $I_s(t)$ enters only through the trajectory of the particle $I_s(t) = I_s(\vec{R}(t))$. The temporal intensity correlation, which is the measured quantity, is then determined solely by the dynamics of the particle. To see this, we expand a general intensity distribution $I(\vec{r})$ in the vicinity of its peak:

$$I(\vec{r}) \simeq I_0 + \frac{1}{2}\sum_i \left(\frac{\partial^2 I}{\partial r_i^2}\right)_0 r_i^2 = I_0\left(1 - \sum_i \frac{r_i^2}{2\omega_i^2}\right),$$

where $i = x, y, z$ and ω_i are the widths of the intensity distribution around the peak in the three directions. The scattered ACF for a particle located at $\vec{r} = \vec{R}(t)$ is therefore given by the time average:

$$\langle I_s(0)I_s(t)\rangle \simeq I_0^2\left[\left(1 - \frac{1}{2}\sum_i \frac{\langle R_i^2\rangle}{\omega_i^2}\right)^2 + \frac{1}{4}\sum_i \frac{1}{\omega_i^4}(\langle R_i^2(t)R_i^2(0)\rangle - \langle R_i^2\rangle^2)\right], \quad (1)$$

where $\langle R_i^2\rangle = \langle R_i^2(t)\rangle$ is time independent. In the case where $R_i(t)$ obeys Gaussian statistics, we have $\langle R_i^2(t)R_i^2(0)\rangle - \langle R_i^2\rangle^2 = 2\langle R_i(t)R_i(0)\rangle^2$, and hence the ACF is directly related to the position correlation function of the center of mass of the particle.

In this section we first apply these ideas for the particular case of a Gaussian beam. We calculate explicitly the intensity ACF of a point particle exhibiting Brownian motion confined inside a harmonic potential well. We then consider the finite size effects of the scatterer on the ACF, and show that they introduce corrections to the leading temporal dependence, which remains that of a point particle.

A point particle in a focused beam

Consider scattering by a particle subject to an inhomogeneous light illumination whose intensity we model by Gaussian functions:

$$I(\vec{r}) = I_0 \prod_i \exp(-r_i^2/2\omega_i^2), \quad (2)$$

where $\vec{r} = \vec{R}(t)$ is the position of the point scatterer. The time dependence of the scattered intensity enters implicitly only through the trajectory of the point particle $I_s(\vec{R}(t))$. Equation 2 is a convenient approximation of the actual shape of a focused Gaussian beam that is a Lorentzian in the $\hat{z}$ direction and Gaussian in the $\hat{x}$-$\hat{y}$ plane (Yariv, 1991). Note that we are interested in small particle displacements around the center of the intensity distribution for which a Gaussian distribution in $\hat{z}$ gives essentially the same dynamics in the ACF. Our prediction for the ACF can be generalized to account for a Lorentzian in the $\hat{z}$ direction, which would involve more cumbersome expressions without any new essential information. It follows from Eq. 2 that the ACF is

$$\langle I_s(0)I_s(t)\rangle = I_0^2\left\langle \prod_i \exp\left[-\frac{R_i^2(0) + R_i^2(t)}{2\omega_i^2}\right]\right\rangle.$$

In the last equation we choose the components of $\vec{R}(t)$ to be collinear with the principal axes of the beam, so that we can replace the average of the product by the product of the averages. To evaluate each average, we make use of the symmetrized variables, $R_{i\pm}(t) = [R_i(t) \pm R_i(0)]/\sqrt{2}$, which are uncorrelated, and $\langle R_{i+}(t)R_{i-}(t)\rangle = 0$. This property enables a further decoupling into a product of two single Gaussians in each direction:

$$\left\langle \exp\left[-\frac{R_i^2(0) + R_i^2(t)}{2\omega_i^2}\right]\right\rangle = \left\langle \exp\left[-\frac{R_{i+}^2(t)}{2\omega_i^2}\right]\right\rangle\left\langle \exp\left[-\frac{R_{i-}^2(t)}{2\omega_i^2}\right]\right\rangle.$$

The stochastic variables $R_{i\pm}(t)$ obey a Gaussian probability distribution, $P(R_{i\pm}(t)) = (2\pi\langle R_{i\pm}^2(t)\rangle)^{-1/2}\exp[-R_{i\pm}^2(t)/2\langle R_{i\pm}^2(t)\rangle]$, where $\langle R_{i\pm}^2(t)\rangle$ are the mean squares of $R_{i\pm}(t)$. Using this distribution to calculate the decoupled statistical averages, one gets

$$\langle I_s(0)I_s(t)\rangle = I_0^2 \prod_i \frac{S_i - 1}{\sqrt{S_i^2 - \langle R_i(t)R_i(0)\rangle^2/\langle R_i^2\rangle^2}}, \quad (3)$$

where $S_i = 1 + \omega_i^2/\langle R_i^2\rangle$ is a measure of the beam width relative to the particle mean square amplitude (we note in a previous publication a change from our notation used to define S_i; Bar-Ziv et al., 1997). It is common to normalize the ACF by its value at infinity ($t \to \infty$):

$$g(t) \equiv \frac{\langle I_s(0)I_s(t)\rangle}{\langle I_s\rangle^2} = \prod_i \frac{S_i}{\sqrt{S_i^2 - \langle R_i(t)R_i(0)\rangle^2/\langle R_i^2\rangle^2}} \quad (4)$$

assuming that $\langle R_i\rangle = 0$. The normalized amplitude of the signal is then

$$\beta \equiv g(0) - 1 = \prod_i \left(\frac{S_i}{\sqrt{S_i^2 - 1}}\right) - 1.$$

For small particle excursions with respect to the beam waist, $\omega_i^2/\langle R_i^2\rangle \gg 1$, we have $\beta \approx \frac{1}{2}\Sigma_i\langle R_i^2\rangle^2/\omega_i^4$, and for the other extreme of $\omega_i^2/\langle R_i^2\rangle \ll 1$, $\beta \approx \Pi_i(\langle R_i^2\rangle/2\omega_i^2)^{1/2}$, which is the ratio between the fluctuation volume and the volume of illumination. Thus the amplitude of the signal is enhanced for strongly focused beams and for large mean square amplitudes. This result is applicable only for a point particle. For finite-sized particles, β is affected by the form factor, as we discuss below (under Effects of the Particle Form Factor).

A Brownian particle in a harmonic potential

Consider a particle exhibiting Brownian motion inside a harmonic potential, which could be formed, for example, by laser tweezers or by a macromolecule anchored on one side to the particle and on the other side to a rigid surface, whose force constant we wish to measure. We assume that the principal axes of the potential are collinear with the illuminating beam. To calculate the scattered ACF of this confined particle, we introduce its stochastic equation of motion, neglecting the inertial term that would give rise to a fast time scale $\tau = m/\zeta$ (shorter than 1 μs for micron-sized silica particles):

$$\kappa_i R_i + \zeta \dot{R}_i = f(t).$$

Here κ_i is the force constant proportional to the second derivative of the potential, expanded about its minimum; ζ is the friction coefficient; and $f(t)$ is a stochastic uncorrelated thermal force,

$$\langle f(t)f(t')\rangle = 2\zeta k_B T\delta(t-t'), \quad \langle f(t)\rangle = 0.$$

The correlation function of the position, $R_i(t)$, decays exponentially:

$$\langle R_i(0)R_i(t)\rangle = \langle R_i^2\rangle \exp(-t/\tau_i) \tag{5}$$

where

$$\tau_i = \frac{\zeta}{\kappa_i}$$

and the mean square amplitude is $\langle R_i^2\rangle = k_B T/\kappa_i$. Here T is the temperature, k_B is the Boltzmann constant, and $\zeta = 6\pi\eta a$, where a is the radius of the particle and η is the viscosity of the surrounding solution (Doi and Edwards, 1988; Chaikin and Lubensky, 1995). The decay time τ_i is also the time it takes the particle to diffuse over a distance equal to the mean square amplitude, $\langle R_i^2\rangle = D\tau_i$, where $D = k_B T/\zeta$ is the diffusion coefficient. Using the position correlation function (Eq. 5), the normalized ACF (Eq. 4) becomes

$$g(t) = \prod_i \frac{S_i}{\sqrt{S_i^2 - \exp\left(-\frac{2t}{\tau_i}\right)}}. \tag{6}$$

For a strong restoring force, the fluctuations are smaller than the beam size, $S_i \gg 1$, and the ACF can be approximated by a sum of exponential functions:

$$g(t) \approx 1 + \frac{1}{2}\sum_i \left(\frac{\langle R_i^2\rangle}{\omega_i^2}\right)^2 \exp\left(-\frac{2t}{\tau_i}\right). \tag{7}$$

Equation 7 is identical to Eq. 1, obtained for a general quadratic intensity distribution when substituting the position correlation of the Brownian particle. This is the limit where the particles perform small excursions, and hence the Gaussian beam is approximated by a parabolic profile. In the case of strong fluctuations or a weak potential, $S_i \to 1$, and the general ACF (Eq. 3) goes to zero as $t \to \infty$. We therefore cannot normalize the ACF, which takes the following form:

$$\langle I_s(0)I_s(t)\rangle \simeq I_0^2 \prod_i \left(\frac{2\omega_i^2}{\langle R_i^2\rangle}\right)^{1/2} \prod_i \left(1 + \frac{Dt}{\omega_i^2}\right)^{-1/2}, \tag{8}$$

which decays as $t^{-3/2}$ at long times. Note that as $t \to \infty$, the ACF signal becomes very weak, $\langle I_s(0)I_s(t)\rangle \to 0$, because the motion takes place mostly outside of the scattering beam. A discussion of the extreme limit of a freely diffusing particle and the experimental procedure used to enhance the signal in this case is given in the Results section (under The Diffusive Limit).

Effects of the particle form factor

The previous discussion of the time dependence of the correlation function was based on a model of a fluctuating point particle. For a finite body, the entire volume of the object contributes to the scattering, and this may change both the wavevector as well as the time dependence of the intensity autocorrelation function. Below we derive an expression for the LDLS intensity for scattering from a finite body. We show that when fluctuations of the center of mass are small compared to the linear dimensions of the body and to the optical wavelength, the scattering can be written as the product of the LDLS intensity for a point particle, multiplied by a form factor that takes into account the spatial inhomogeneity of the laser beam. When this form factor vanishes, higher order terms in the position of the center of mass must be taken into account, and this changes quantitatively the time decay of the intensity correlations.

The intensity-intensity ACF is proportional to

$$\langle I_s(t)I_s(0)\rangle \approx \langle E_s(0)E_s^*(0)E_s(t)E_s^*(t)\rangle$$

where $E_s(t)$ is the scattered electric field and the average is over the fluctuations of the particle. At a distance d in the far field, $E_s(t)$ is given by (Berne and Pecora, 1976)

$$E_s(t) = \frac{e^{ik_1 d}}{d}\int e^{-i\vec{q}\cdot\vec{r}} A(\vec{q})\,d\vec{r}\,d\vec{q}$$

where $\vec{r}$ is the distance from the origin, defined by the incoming beam focal point, to a point within the scatterer. $A(\vec{q})$ is the Fourier transform of the incoming Gaussian field, $A(\vec{q}) \approx \exp(-(\vec{q}-\vec{q}_0)^2\omega^2/2)$, where $\vec{q}_0 = \vec{k}_0 - \vec{k}_{10}$ is the primary scattering wavevector, $\vec{k}_{10}$ is the incoming wavevector along the axis of the beam, and $\vec{k}_0$ is the outgoing wavevector in the direction of the observer. The factor in front of the integral gives a constant amplitude, which we omit hereafter. The integrals extend over the volume of the body and over the scattering wavevectors.

After transforming to the center of mass position $\vec{R}(t)$ using $\vec{\rho} = \vec{r} - \vec{R}(t)$, and integrating over q-space, we obtain

$$E_s(t) \sim \exp\left(-i\vec{q}_0 \cdot \vec{R}(t) - \frac{R^2(t)}{4\omega^2} F(\vec{q}_0, \vec{R}, (\omega))\right), \quad (9)$$

where the scattered field of a point particle is multiplied by $F(\vec{q}_0, \vec{R}, \omega)$ in which finite size effects are lumped in

$$F(\vec{q}_0, \vec{R}(t), \omega) = \int_v d\vec{\rho} \exp(i\vec{q}_0 \cdot \vec{\rho}) \exp\left(-\frac{\rho^2}{4\omega^2}\right) \exp\left(-\frac{\vec{R}(t) \cdot \vec{\rho}}{2\omega^2}\right). \quad (10)$$

We consider here, for simplicity, only the isotropic case, $\omega_i = \omega$, in which the fluctuations of the position of the center of mass are smaller than the particle size or the wavelength of light. Then the last term in $F(\vec{q}_0, \vec{R}, \omega)$ can be expanded as $\exp(-\vec{R}(t) \cdot \vec{\rho}/2\omega^2) \simeq 1 - \vec{R}(t) \cdot \vec{\rho}/2\omega^2 + (\vec{R}(t) \cdot \vec{\rho})^2/8\omega^4$. This is valid for small fluctuations of a large particle, because for most of the integration volume, $a > |\vec{\rho}| \gg |\vec{R}(t)|$, except for a narrow neighborhood around its center, $|\vec{\rho}| \leq |\vec{R}(t)|$, whose contribution to the volume integral is negligible. Integration then yields

$$F(\vec{q}_0, \vec{R}(t), \omega) \simeq F_0(\vec{q}_0, \omega) - \frac{R(t)}{2\omega^2} F_1(\vec{q}_0, \omega) + \frac{R^2(t)}{8\omega^4} F_2(\vec{q}_0, \omega), \quad (11)$$

where $F_0(\vec{q}_0, \omega)$, $\vec{F}_1(\vec{q}_0, \omega)$, and $F_2(\vec{q}_0, \omega)$ are the moments of the form factor:

$$F_n(\vec{q}_0, \omega) = \int_V d\vec{\rho} \left(\vec{\rho} \cdot \frac{\vec{R}(t)}{R(t)}\right)^n \exp(i\vec{q}_0 \cdot \vec{\rho}) \exp\left(-\frac{\rho^2}{4\omega^2}\right).$$

The first term of the expansion contains the usual phase of a plane wave and an additional Gaussian dependence due to field inhomogeneity. For a spherical particle of radius a, one can write it as

$$F_0 = 4\pi \int_0^a \frac{\rho \sin(q_0\rho)}{q_0} \exp\left(-\frac{\rho^2}{4\omega^2}\right) d\rho. \quad (12)$$

In the limit of a small particle, $a \ll \omega, \lambda$, $F_0 = V$, whereas for $a \to \infty$, $F_0 = 4\sqrt{\pi}\omega^3 \exp(-q_0^2\omega^2)$.

The resulting form factor, F_0, shows deep minima (nodes) as a function of the scattering wavevector, q_0. Near these nodes, the terms proportional to $\vec{R}$ and $\vec{R}^2(t)$ in the expansion (Eq. 11) should be taken into account. Then the temporal dependence of the ACF is modified, because of the explicit dependence of $F(\vec{q}_0, \vec{R}, \omega)$ on $\vec{R}(t)$. Outside the vicinity of the nodes, the finite body contribution is manifested through a constant form factor, which does not alter the temporal behavior.

Dumbbell model

In principle, one can proceed and obtain the full ACF for a sphere using the above scattered fields. However, this involves cumbersome calculations. Instead we chose to present the essential physics by considering the simple model case of a dumbbell. This model, which is solved analytically, provides the finite size and large displacement corrections to the dynamics of the ACF. In addition, one can estimate the theoretical value of the signal-to-noise ratio β and show that it is maximized in the vicinity of a scattering node.

Consider two point particles located at the ends of a rod of fixed length $2l$. For simplicity, we restrict their motion to one dimension along the rod axis, inside a beam whose profile is given by $I \approx \exp(-x^2/2\omega^2)$. The only degree of freedom of this system is the position of the rod center, $R(t)$, which determines the positions of the two point scatterers, $R_{1,2}(t) = R(t) \pm l$. The scattered fields from the two particles are $E_i \approx \exp(-i\vec{q} \cdot \vec{R}_i)\exp(-R_i^2/4\omega^2)$, where $\vec{q}$ is the scattering vector. The total intensity is then given by

$$I_s \sim |E_1 + E_2|^2 \sim \exp\left(-\frac{R^2}{2\omega^2}\right)\exp\left(-\frac{l^2}{2\omega^2}\right) \cdot \left[\cosh\left(\frac{Rl}{\omega^2}\right) + \cos(2ql)\right]. \quad (13)$$

The first exponent is the point-particle contribution due to the motion of the center of mass inside the beam. The other terms account for the phase interference, which vanishes for one particle, $l = 0$. The scattered dumbbell intensity is not isotropic, as for a point particle, and contains an angular dependence $\cos(2ql)$.

To calculate the ACF we need to calculate averages, using the particle probability function, just as for a point particle. The result is

$$\langle I_s(0)I_s(t)\rangle \sim \frac{S-1}{\sqrt{S^2-\Delta^2}} e^{-l^2/2\omega^2}([\cos(2ql) + e^{\Phi}]^2 + 2e^{\Phi}\sinh^2(\Phi \cdot \Delta)) \quad (14)$$

where $\Delta(t) = \langle R(t)R(0)\rangle/\langle R^2\rangle$ and

$$\Phi(t) = \frac{l^2}{2\omega^2}\frac{S-\Delta^2}{S^2-\Delta^2}.$$

Notice that the prefactor is the point particle ($l = 0$) ACF (Eq. 3). The first term accounts for the angular dependence, and the others are exponential functions of combinations of the position correlation function, $\Delta(t)$, which introduce higher harmonics of the basic time scales, τ_i.

In the small fluctuation limit, $R^2, Rl \ll \omega^2$, the scattered intensity can be approximated by

$$I_s \sim \cos^2(ql) + \frac{R^2}{2\omega^2}\left(\frac{l^2}{2\omega^2} - \cos^2(ql)\right).$$

The angular part of I_s exhibits nodes at $ql = (ql)_n = (n + 1/2)\pi$. At angles far from a node, $\cos^2(ql) \gg l^2/\omega^2$, and the leading behavior is that of a point particle, $I_s \approx 1 - R^2/2\omega^2$. However, in the vicinity of a node, the leading term is $I_s \approx l^2R^2/4\omega^4$, and the ACF scales like $\langle R^2(t)R^2(0)\rangle$. The resulting ratio of the time-dependent part of the ACF to its DC value β behaves like

$$\beta \equiv \frac{\langle I_s(0)^2\rangle}{\langle I_s\rangle^2} - 1 = 2\left[1 + \frac{2\omega^2}{\langle R^2\rangle}\frac{\cos^2(ql)}{l^2/2\omega^2 + \cos^2(ql)}\right]^{-2}. \tag{15a}$$

In the vicinity of a node, β is maximized to a value independent of the beam geometry $\beta_n = 2$. Far from the node this value reduces to the point particle value $\beta_0 = \langle R^2\rangle^2/2\omega^4$. The width of the angular range where the node dominates is $q - q_n \simeq \sqrt{\langle R^2\rangle}/\omega^2$.

EXPERIMENTAL SET-UP

A complete scheme of the experimental set-up has been given by Bar-Ziv et al. (1997). Spherical silica beads suspended in water were trapped by a strongly focused laser beam with a spot of dimensions L_i and tunable intensity I_T. The optical tweezers were set up using an inverted microscope, a high numerical aperture lens, and a 514.5-nm green argon laser. To independently control the trap force and the scattering intensity, we used a red (632.8 nm) HeNe laser, collinear with the green laser, as the scattering light source. The ratio of intensities of the two lasers was less than 1/100, and hence the trapping effect of the weaker red laser could be neglected. A 632.8-nm line filter in front of our detector ensured that only the red light was actually probed. The scattered light was collected by specially designed probes. These probes are based on bare single mode optical fibers that are treated to tailor their numerical aperture and thickness to the desired application. For example, we reduced the outer diameter of the fiber to be able to locate the probe at a shallow angle with the incident direction and pick up light scattered by a scatterer localized close to the bottom coverslip. In addition, one can fine-tune the numerical aperture of the probe by treating the fiber surface so that light is collected selectively from the scattering particle (Meller, 1997).

Fine adjustments of the probe enabled by a sensitive micromanipulator were carried out to optimize the signal-to-noise ratio. We were able to reach very high signal-to-noise ratios by positioning the optical fiber outside the light cone defined by the incoming beam, so that only scattered light was collected. The distance of the fiber tip from the localized scatterer was $\sim$100 μm away from the optical axis, forming a 75° angle with the incident direction.

The scattered intensity collected by the fiber was fed into a photomultiplier tube (PMT) and transferred to a correlator, which calculated the ACF. A few minutes was typically sufficient to obtain a smooth ACF at a count rate of 20 kHz. The level of the normalized baseline is on the order of 10^{-3}, giving a dynamic range of 2.5–3 decades. Our time resolution was extended down to $\sim$20 ns by cross-correlation of the signal with itself by the use of two PMT detectors. It was absolutely necessary to minimize low-frequency noise, which increases the background level. This was done by 1) measuring inside a rigid chamber that is stable against mechanical vibrations, 2) coupling the laser into single mode fibers to reduce mechanical and pointing instabilities, and 3) averaging many times over the integration period to avoid low-frequency mechanical drifts. Because we scattered a strongly focused light beam, the main contribution to the signal came only from the localized illuminated region. However, it was difficult to avoid stray light from back reflections, which increased the background level and reduced the signal-to-noise ratio. To minimize this, our measuring chamber was made of a light-absorbing material.

RESULTS

Single particle in a harmonic potential

We demonstrate LDLS by applying it to a spherical bead held in an optical trap. For small displacements, the potential well formed by the green laser is approximately harmonic, with a restoring force $-\kappa_i r_i$ acting on the particle. The spring constant is proportional to the trap intensity I_T. The motion is overdamped by the viscous fluid, with an exponential time scale given by $\tau_i = 6\pi a\eta/\kappa_i$.

A typical ACF of a silica bead in an optical trap is shown in Fig. 1. The main feature of this ACF is the existence of two distinct exponential decay times (see *inset*), which we attribute to the motion of the particle along the longitudinal and transverse directions in the three-dimensional trap. The low baseline level and the relatively high intercept (typically in our experiments, $\beta \geq 0.5$) result in a wide dynamic

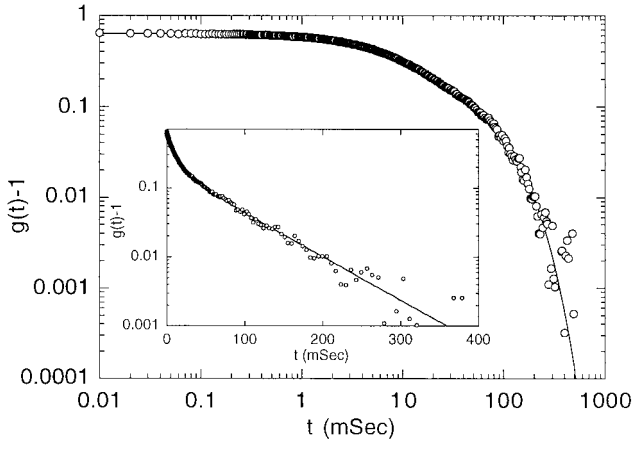

FIGURE 1 A typical ACF of a trapped particle measured by LDLS. The log-log plot manifests the relatively large signal-to-noise ratio of the ACF and the extended time range accessible by this method. In the inset the same ACF is plotted on a semilog scale, to highlight the two exponential decay times that correspond to motions in the axial and transverse directions (Bar-Ziv et al., 1997).

range, which provides a reliable determination of the well-separated time scales. We fit our data to Eq. 6, leaving as free parameters the exponential time scales and their amplitudes. Equation 6 is the ACF of a harmonic pointlike particle, which is the leading term for a finite-sized particle.

Fig. 2 shows a plot of one over the two time scales obtained from the fits as a function the force constant κ. To obtain this plot we measured the time scales as a function of trap intensity, yielding $\tau_i \propto 1/I_T$ (Bar-Ziv et al., 1997). Using the relation $\tau = \zeta/\kappa$, we obtain the values of the force constants κ as a function of laser intensity I_T for both time scales, with the known value of ζ. The longer time scale (*squares*) corresponds to motion in the longitudinal direction, whereas the shorter time scale (*circles*) is related to the transverse motion.

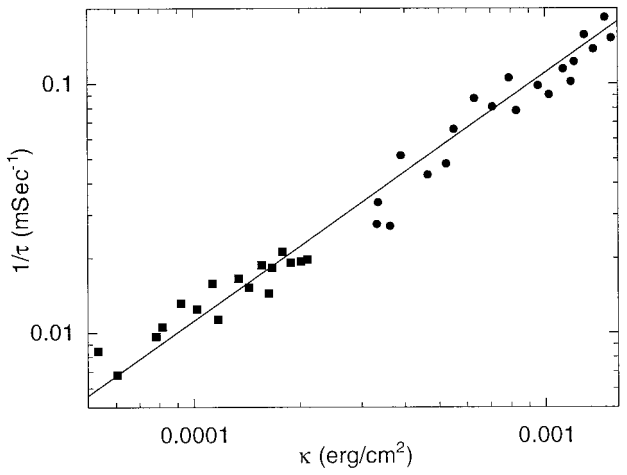

FIGURE 2 Plot of the inverse time scales for the axial (■) and transverse (●) motion of the particle in the three-dimensional potential well as a function of force constant κ (Bar-Ziv et al., 1997). The data were obtained by first measuring a linear dependence of the inverse time scales as a function of laser intensities and then converting to force constants, using the relation $\tau = 6\pi\eta a/\kappa$ (see text).

Scattering from two particles

We demonstrate the ability of LDLS to probe dynamics of particles that have additional degrees of freedom by scattering from a pair of identical beads in contact in the trap. These additional degrees of freedom show up as new time scales in the measured ACF.

A simple argument shows that the minimum energy configuration of the system is that of one bead located close to the center of the trap while the other one is adjacent in the $\hat{z}$ direction. Because the beads are in contact, we expect four distinct modes, namely, two translations of the pair along the transverse and longitudinal axes and two rotations of the pair axis, θ and φ, respectively. The translations of the center of mass exhibit overdamped harmonic motion and hence should show up as two distinct exponential time scales in the ACF, as in the single-particle case. The motion of the angle θ formed by the pair axis relative to the beam axis is also overdamped, but with a force constant that is weaker than the translational force constants (Meller, 1997). Finally, the rotation of the azimuthal angle φ is unconstrained because of the cylindrical symmetry of the trap, and hence a freely diffusive soft mode should be observed with a typical rotational diffusion coefficient of $\Theta \leq 0.1$ rad/s. This implies a time scale of a few tens of seconds, which is beyond the limit of our detection in this experiment.

Fig. 3 shows an ACF of a pair of beads in contact, 1 μm in diameter, with three exponential decay times, in contrast to the single-particle ACF (Fig. 1), which has only two time scales. We attribute the first two time scales, of 4 and 20 ms, to the motion of the center of mass, and the third, of 2.4 s, to the fluctuations of the angle θ. The latter time scale is indeed significantly longer than the first two.

The diffusive limit

One expects a qualitatively different ACF for a freely diffusive particle because there is no restoring force and the relevant length scale is time dependent, $\sqrt{Dt}$. A single freely diffusing particle will remain in the illuminated region during a time period of $\tau_D = \omega^2/D$, which is too short to obtain enough statistics for a reliable ACF. We thus conducted the following experiment: a single bead was held in a strong trap and then released, at which point the integration of the ACF over an integration time $T \gg \tau_D = \omega^2/D$, on the order of 10 s, was started. This procedure was repeated $N \approx 150$ times, which was sufficient to obtain enough statistics. The averaged ACF is shown in Fig. 4.

To calculate the theoretical ACF for this experiment, one must replace the time average over the motion of a single particle with an ensemble average of many free particle events measured during a finite period T. Notice that in this formulation of the problem, the statistical ensemble no

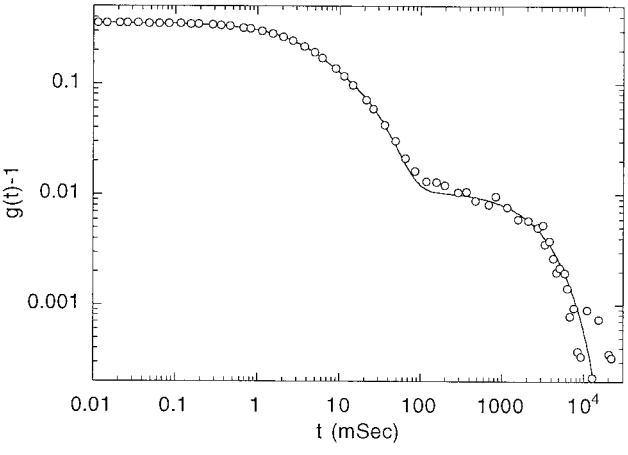

FIGURE 3 Intensity autocorrelation function measured for a pair of identical particles in an optical trap fitted (*solid line*) to three exponential decay times: 3.8, 21, and 2400 ms. The first two correspond to motion of the center of mass, and the third is related to fluctuations of the axis angle θ.

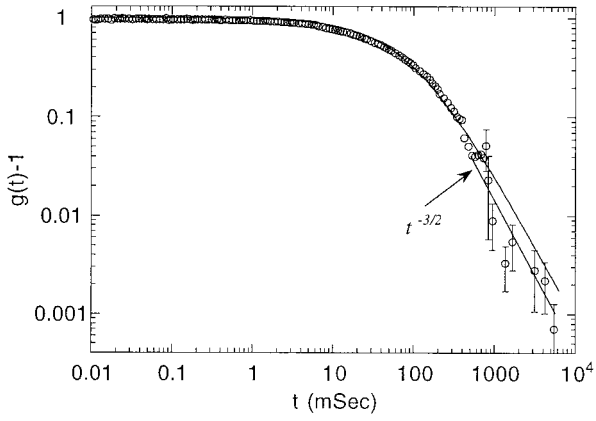

FIGURE 4 Averaged intensity ACF measured for a free (diffusive) particle using the procedure described in the text. At long times the ACF decays as $t^{-3/2}$, as expected from Eq. 16. The data are normalized to unity and fitted as described in the text.

longer has time translational invariance, $\langle I(0)I(t)\rangle \neq \langle I(\tau)I(\tau + t)\rangle$, because for each measurement of the ACF, the particle was located near the center of the trap at $t = 0$. We reconstruct the measured ACF of diffusing particles by averaging the signal over the ensemble of N experiments:

$$\langle I_s(0)I_s(t)\rangle = \frac{1}{N}\sum_n \frac{1}{T}\int_0^T I_{s,n}(t')\, I_{s,n}(t + t')\mathrm{d}t'.$$

When N is large enough, one can replace the sum over N by the statistical average over the single particle Gaussian distribution function,

$$\langle I_s(0)I_s(t)\rangle = \frac{I_0^2}{T}\int_0^T \prod_i \left\langle \exp\left(-\frac{r_i^2(t')}{2\omega_i^2}\right)\exp\left(-\frac{r_i^2(t + t')}{2\omega_i^2}\right)\right\rangle \mathrm{d}t'. \tag{16}$$

Averaging and integrating the last expression for the case of azimuthal symmetry, we get

$$\langle I_s(0)I_s(t)\rangle = I_0^2\Gamma(t)\prod_i\left(\frac{\omega_i^2/4DT}{1 + Dt/\omega_i^2}\right)^{1/2}, \tag{17}$$

where $\Gamma(t)$ is a slowly varying function of t and i denotes the coordinates ρ and z (Meller, 1997). We note that the long-time behavior of the ACF (Eq. 17) is a power law, $t^{-3/2}$.

To compare this prediction to our measured ACF (Fig. 4), we note that our measurements always consist of a nonzero background term, which we did not account for in Eq. 17. We therefore added this experimental baseline to the theoretical expression and normalized both the experimental data and Eq. 17 to unity at the shortest measured time. Our data were best fitted over the entire range, using Eq. 17 with $\omega_x = \omega_y = 0.15$, $\omega_z = 0.50$ μm (actual spot dimensions are larger by $\sqrt{2\log 2}$), with $D = 4.4 \times 10^{-9}$ cm^2/s, the diffusion constant for the 1-μm beads used in this experiment. The integration time was $T = 7$ s. We note that the long-time behavior of this ACF is qualitatively different from an ACF of a trapped bead (see Fig. 1), because the data approach $t^{-3/2}$, as shown in Fig. 2 and predicted by Eq. 17.

DISCUSSION

We have presented a new quantitative tool for studying the dynamical behavior of single objects in the colloidal and biological realm. The basic concept is to perform a dynamic light scattering experiment with a single scatterer under the microscope, using focused laser light. For this purpose we developed a new probe based on optical fibers that enables one to collect light under the microscope at different scattering angles. The light is detected by a PMT coupled to our optical fiber probe, and the signal is fed into a digital correlator that calculates the intensity autocorrelation function. Using the intensity ACF, one obtains the dynamic spectrum of a fluctuating object over many decades in time down to the nanosecond regime.

Scattering with inhomogeneous illumination has a twofold advantage. First, one can scatter light from a specific object or localized region within the field of view of the microscope, with a spatial resolution exceeding that of conventional optical techniques. The second advantage is that the precise knowledge of the spatial form of the incident scattering light allows for theoretical prediction of the scattering correlation function. We have presented a theoretical framework for calculating the ACF of a single rigid scatterer by the use of Gaussian illumination. One can now extend the theory to particles with internal degrees of freedom, such as membranes, or to intensity profiles other than Gaussian, such as evanescent fields.

We demonstrated the feasibility of the technique with a simple model experiment of a single Brownian particle (a spherical glass bead) in a harmonic potential formed by an optical trap. The motion of this particle in the well is overdamped with a time scale given by the ratio of the drag force and the harmonic spring constant of the potential. 1) By changing the intensity of the trapping laser, we varied the force constant of the potential and measured the characteristic decay times of the ACF. These decay times are inversely proportional to the intensity, as expected from theory. 2) For a given trapping intensity, we measured two decay times in the ACF, corresponding to motion in the two different directions of the anisotropic optical trapping potential, which dictate different force constants for the transverse and longitudinal directions. 3) For a diffusive particle, we measured an asymptotic power-law decay of the ACF, which is different from the exponential decay characterizing a trapped particle. 4) To extend the measurements to more complex objects, we trapped two particles in contact and obtained an ACF that exhibits the various degrees of motion of the pair, namely the translations of the center of mass and the fluctuations of the pair axis.

We emphasize two important experimental aspects of LDLS. Our ability to manipulate the optical fiber probe

away from the incoming beam enables us to optimize the signal-to-noise ratio. Our spatial resolution is primarily determined by the beam gradient, and not by optical phase shifts, as in ordinary light scattering techniques. One can greatly improve the spatial resolution by scattering from steeper gradients along the beam profile. New possible applications of LDLS could be for the measurement of 1) Elasticity of molecular springs attached to beads such as proteins and DNA, 2) fluctuations of single vesicles or cells subjected to an external field such as tension, 3) scattering from a fluctuating single particle embedded in a complex medium, such as an actin network or the interior of a cell, to probe the viscoelastic properties of this medium. Such novel experiments await future work.

We acknowledge useful discussions with E. Bar-Ziv, P. Chaikin, D. Chatenay, E. Domany, T. Kam, Y. Silberberg, and D. Weitz.

AM acknowledges support from the Israeli Ministry of Science and the Arts. This work was supported in part by the Israeli Ministry of Science and the Arts (grant 5879); the Minerva Foundation, Munich; and the Minerva Center for Nonlinear Science.

REFERENCES

Ashkin, A. 1980. Applications of laser radiation pressure. *Science.* 210: 1081–1088.

Ashkin, A., D. J. M., and T. Yamane. 1987. Optical trapping and manipulation of single cells using infrared laser beams. *Nature.* 330:769–773.

Bar-Ziv, R., A. Meller, T. Tlusty, E. Moses, J. Stavans, and S. A. Safran. 1997. Localized dynamic light scattering: probing single particle dynamics at the nanoscale. *Phys. Rev. Lett.* 78:154–157.

Berne, B. J., and R. Pecora. 1976. Dynamic Light Scattering with Application to Chemistry, Biology and Physics. Wiley, New York.

Chaikin, P. M., and T. C. Lubensky. 1995. Principles of Condensed Matter Physics. Cambridge University Press, Cambridge.

Chu, B. 1991. Laser Light Scattering, Basic Principles and Practice. Academic Press, San Diego.

Doi, M., and S. F. Edwards. 1988. The Theory of Polymer Dynamics. Clarendon Press, Oxford.

Finer, J. T., R. M. Simmons, and J. A. Spudich. 1994. Single myosin molecule mechanics: piconewton forces and nanometer steps. *Nature.* 368:113–118.

Kuo, S. C., and M. Sheetz. 1993. Force of single kinesin molecules measured with optical tweezers. *Science.* 260:232–234.

Meller, A. 1997. Ph.D. thesis. Weizmann Institute of Science, Rehovot, Israel.

Simmons, R. M., J. T. Finer, S. Chu, and J. A. Spudich. 1996. Quantitative measurements of force and displacement using an optical trap. *Biophys. J.* 70:1813–1822.

Svoboda, K., and S. M. Block. 1994. Biological applications of optical forces. *Annu. Rev. Biophys. Biomol. Struct.* 23:247–285.

Svoboda, K., P. P. Mitra, and S. M. Block. 1994. *Proc. Natl. Acad. Sci. USA.* 91:11782.

Svoboda, K., C. F. Schmidt, D. Branton, B. J. Schnapp, and S. M. Block. 1993. Direct observation of kinesin stepping by optical trapping interferometry. *Nature.* 365:721–727.

Yariv, A. 1991. Optical Electronics. HRW Saunders College Publishing, Chicago.

Yin, H., M. D. Wang, K. Svoboda, R. Landick, S. M. Block, and J. Gelles. 1995. Transcription against an applied force. *Science.* 270:1653–1657.